1

Soft Composites with Tunable Optical and Electrical Properties

Luca Valentini[1] *and Nicola Pugno*[2,3,4]

[1] *University of Perugia, Civil and Environmental Engineering Department, UdR INSTM, Strada di Pentima 4, 05100 Terni, Italy*
[2] *University of Trento, Laboratory of Bio-Inspired and Graphene Nanomechanics, Department of Civil, Environmental and Mechanical Engineering, Trento, Italy*
[3] *Queen Mary University of London, School of Engineering and Materials Science, Mile End Road, London, UK*
[4] *E. Amaldi Foundation, Italian Space Agency, Ket Lab, via del Politecnico snc, 00133 Roma, Italy*

1.1 Introduction

The complexity and integration demands of modern electronics require innovative materials addressing the requirements of flexibility and functionality in terms of electrical or optical properties [1–3]. One of the main challenges is to combine two properties that are mutually exclusive in flexible electronics applications, such as stretchability and low electrical resistance. Elastomeric conductive composites have shown promise for sustainable high-strain and recoverable conductivity [4–6].

Integrating stretchable and electrical conductivity functionalities in an electrode material is advantageous for many electronics applications, such as wearable and printable electronics. Examples of such multifunctional conductive materials exist in the literature and their elastic recovery has been demonstrated for stretch ratios beyond $\lambda > 3$ ($\lambda =$ final length/initial length) [7, 8]. These promising and resilient composites show recoverable performance under cyclical strain, are attractive for tissues that are flexible, and are subjected to large deformations under mechanical loading [9–12]; quantifying these large strains in real time, such as those taking place in skin and muscles, is very important for mechanical characterization of these tissues toward understanding of their mechanical functions under stress in physiological conditions. In this chapter, we will consider three different classes of soft composites: soft color composites whose light transmittance can be actively tuned and controlled through mechanical stretching; viscoelastic polymers that, coupled with hybrid nanoparticles, can be tuned into long-range ordered structures; and elastomeric conductive composites that are promising for sustainable high-strain and recoverable conductivity.

Flexible Carbon-based Electronics, First Edition. Edited by Paolo Samorì and Vincenzo Palermo.

1.2 Soft Color Composites

Photonic crystals of three-dimensionally (3D) ordered materials have attracted extensive interest because of their possible applications in optical filters, optical switches, waveguides, and low-threshold lasers [13–15]. A serious problem involved in colloidal crystal film assembly is their feeble physical organization. Unfortunately, nanoparticle-filled polymers presented an enhancement of the mechanical properties but with a loss of the packing ordering [16]. Shearing has long been known to induce structural transitions from disorder to order in solutions of colloidal particles [17–19]. Several studies suggested that nanoparticles can be equilibrated with fixed architectures in solvents with different viscosities [20–22]. In this regard, core–shell nanoparticles were employed to produce a dispersion phase of 200-nm-scale hard cross-linked spheres and a continuous phase of a gum-like medium, creating polymer opals [23, 24]. These optical composites behave mechanically like rubbers and exhibit strain-sensitive colors due to Bragg diffraction from the opaline packing of the spheres (Figure 1.1).

Following this idea, a soft optical device can be designed by controlling the optical transmittance mechanically by simple shear. This concept is similar to that of conventional window shutters but comprises an optically clear and soft elastomeric matrix, onto which are embedded a parallel array of thin opaque stiffer platelets that hinder light transmittance. By simply controlling the physical and mechanical parameters of the composite such as the stiffness ratio between the polymer matrix (μ_m) and the platelets (μ_p), μ_p/μ_m, the geometrical disposition of the platelets, θ_i, and their aspect ratio, L_p/t_p, it is possible to control the transparency. Loading the device with shear forces allows the rotation of the initially inclined platelets (Figure 1.2), increasing the transmittance.

1.3 Hybrid Viscoelastic Polymer Composites

Adding graphene to a highly viscoelastic polymer gives a composite with unexpected electromechanical properties characterized by electrical conductivity changes and recovery as the material is strained. These sensitive electromechanical nanocomposites can find applications in a wide range of devices. Parafilm is the most used thermoplastic paraffin material in research laboratories; it is stretchable and soft, and owing to its low melting point it becomes adhesive on applying heat and sticks strongly to the receiving materials. Thus, the self-sticking properties of the Parafilm can be used both to receive nanoparticles on the top side and to adhere with the bottom side to stretchable substrates; this practical approach can be considered for large-scale production of stretchable multifunctional materials where physical properties including the nanoparticle order can be controlled by strain. Coupling nanoparticle latex and graphene with Parafilm and transferring such a composite film on stretchable silicone substrate, the nanoparticle organization can be tuned into long-range ordered structures by stretching the substrate with the electrical conductivity of the coating, which can be also tuned.

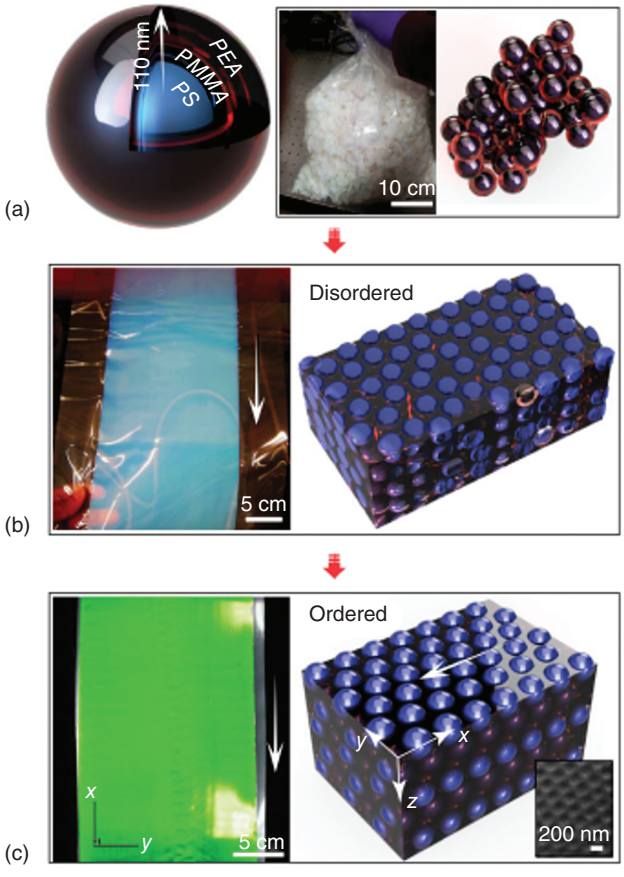

Figure 1.1 (a) PS (polystyrene)–PMMA (polymethyl methacrylate)–PEA (polyethylacrylate) core–shell opaline sphere. (b) The PET–opaline spheres–PET film after rolling lamination; arrow indicates processing direction, with spheres packed randomly. (c) Opaline film with improved sphere packing; arrow indicates shear direction [24].

In a recent experiment, polystyrene (PS) latex/graphene oxide (GO) solutions were drop cast on Parafilm film and left to evaporate at room temperature (Figure 1.3a–c). In order to immobilize the PS sphere on the Parafilm, the substrate was gently annealed at 65 °C. When a rigid sphere is coated with a wetting liquid (i.e. water in our case), the equilibrium of the film is governed by the competing effects of elasticity and capillarity [26]: elasticity tends to keep the film developable while capillarity tends to curve it so as to maximize the area of contact with the sphere. Assuming the GO as an elastic plate of size L, Young's modulus E, Poisson's ratio ν, and thickness h placed onto rigid PS sphere of radius R coated with water (surface tension $\gamma = 72.8\,\mathrm{mN\,m^{-1}}$ at 20 °C), the maximum size in millimeters of complete contact $a_{\max}$ of a strip on a sphere can be more precisely written as $a_{\max} = [(\alpha^*\gamma^*R^4/E^*h) - \beta^*R^{2*}h^2]^{1/4}$ [26], where the constants α and β for a strip are 36 and $3/2(1-\nu)$, respectively. Assuming our GO sheets as strips with an average thickness of about 0.95 nm,

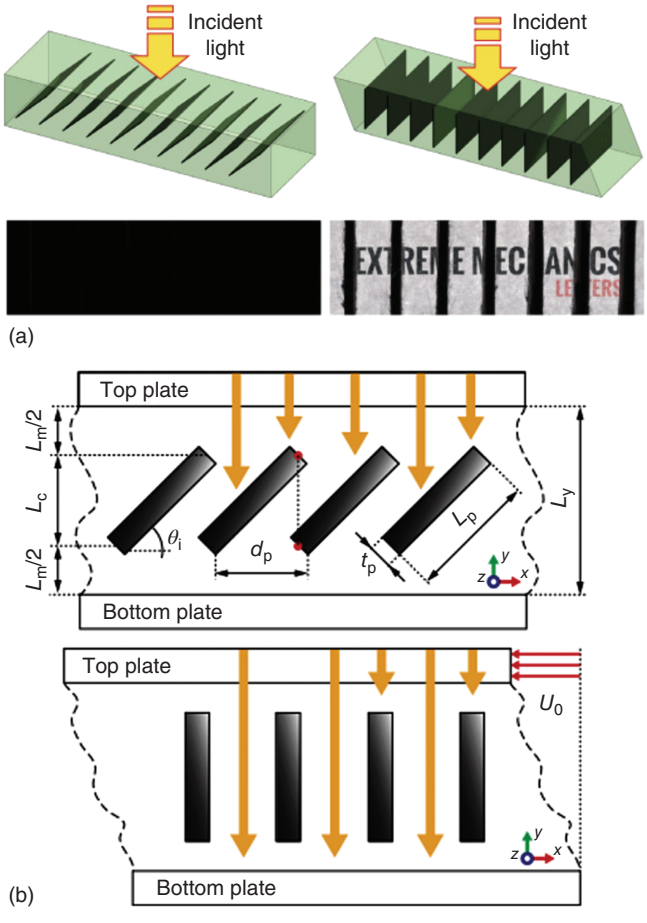

Figure 1.2 Concept of the optical switch: (a) Schematic representation of optical switch device in its undeformed (OFF) and (b) deformed (ON) configurations, respectively. Schematic diagram of the optical switch, indicating all the relevant dimensions. *Source*: López Jiménez et al. 2016 [25]. Reproduced with permission of Elsevier.

Young's modulus of 200 GPa [27], Poisson's ratio of 0.16 [27], and the radius of PS sphere of 50 nm, we obtain a value for $a_{max} \sim 1.70^{*}10^{-5}$ mm. This low value of the contact takes into account the observed crumpled structures in Figure 1.3b.

The electrical resistance in the sample is attributed to the number of percolative graphene contacts. Electrical resistance variation of PS latex/GO/Parafilm film graphene oxideas a function of the stretching ratios, λ, shows that the initial resistance (i.e. unstretched state) increases with the stretching ratio (Figure 1.4). As the composite film was stretched, the resistance was found to increase with the deformation, reaching a maximum value at λ_{max} (i.e. 1.05, 1,2, 1,4, 1,5, 1,6, 1,65, 1,7, and 1,8). Subsequently, as the specimen was brought to the initial state from λ_{max} to 1, the electrical resistance regained the initial values, suggesting an

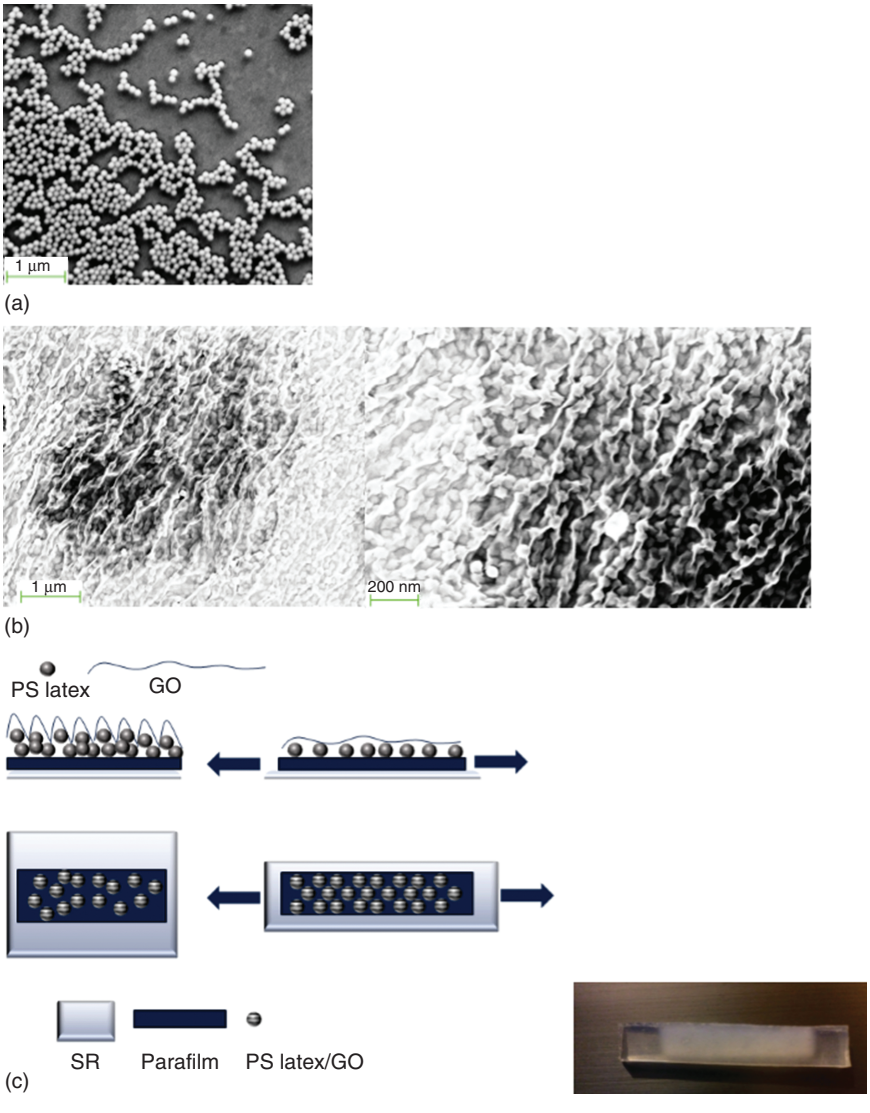

Figure 1.3 Top view FESEM images of (a) PS latex films and (b) PS latex/GO films. (c) Schematic representation of the prepared samples. PS latex spheres at room temperature after drying (bottom panel) leaves disordered spheres stuck to the Parafilm. PS latex spheres after stretching; the arrow indicates the strain direction, with spheres packed ordered. Schematic illustration (top panel) of macroscopic deformation of a graphene sheet on a stretched silicone substrate; first wrinkles form on PS latex spheres, and then unfold as the substrate is strained.

almost reversible mechanism of graphene crumpling previously observed in the stretch axis direction.

Interestingly, once transferred to the Parafilm tape and strained, the composite film shows the appearance of brilliant iridescent bands oriented orthogonal to the strain direction (Figure 1.5a). The formation of such bands is due to a crystalline

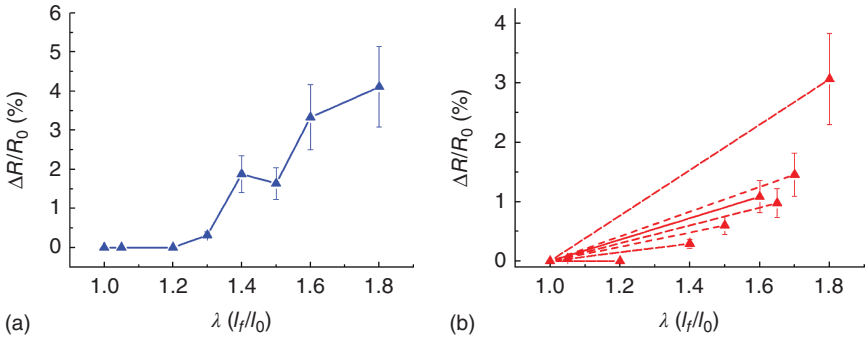

Figure 1.4 (a) Electrical resistance to initial resistance values variations of PS latex/GO/Parafilm coupled with silicone substrate through the stretching and (b) stretching cycles from $\lambda = 1$ to $\lambda_{max} = 1.05$, 1.2, 1.4, 1.5, 1.6, 1.65, 1.7, and 1.8, and then returned to a relaxed state ($\lambda_{max} \rightarrow 1$).

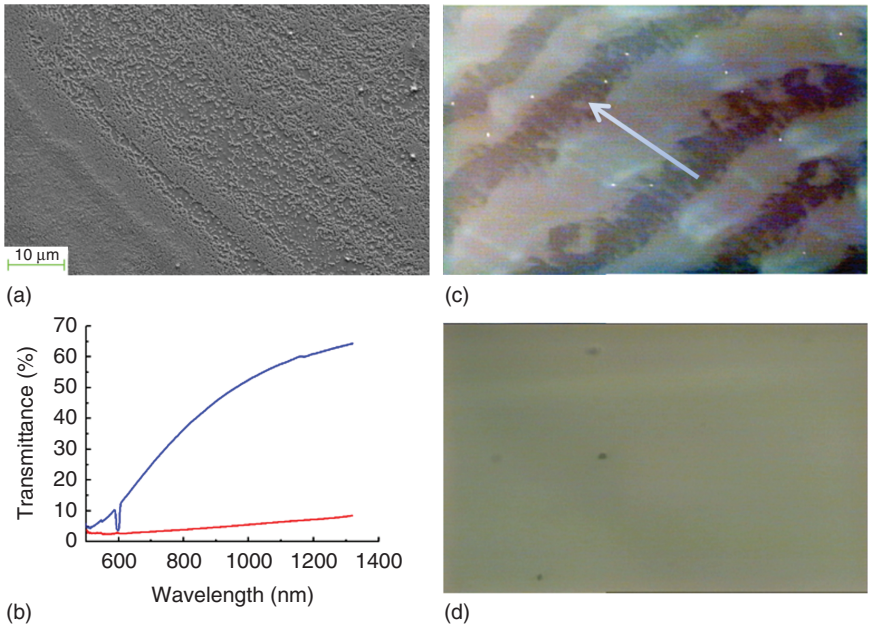

Figure 1.5 (a) FESEM image of the strained PS latex/GO/Parafilm coating. (b) Transmittance of unstrained (red line) and strained (blue line) PS latex/GO/Parafilm coating. Optical micrographs of PS latex/GO/Parafilm sample in (c) stretched and (d) unstretched state, respectively. The arrow indicates the strain direction.

array of colloidal spheres that strongly diffract light of a specific wavelength as determined by the Bragg formula [28, 29]:

$$\lambda_{max} = (8/3)^{1/2} * D(n^2{}_{sphere} * V_{sphere} + n^2{}_{void} * V_{void} - \sin^2\phi)^{1/2}$$

where D is the diameter of the sphere; n_{sphere} and n_{void}, the refractive indices of spheres and voids, respectively, 1.6 for polystyrene spheres and 1 for air voids; V_{sphere} and V_{void} are the volume fractions of spheres and voids in the crystal,

and they are 0.77 and 0.23, respectively; ϕ is the angle between the normal vector of the substrate and the detecting light. We have examined the optical properties of the ordered latex films by measuring their absorption spectra with a UV–vis spectrophotometer. The incident light was perpendicular to the film plane (i.e. $\phi = 0°$). Figure 1.5b shows the absorption spectra of the unstrained and strained latex films, respectively. In its relaxed state, polystyrene latex has no detectable absorption; it is well known that a completely disordered latex arrangement does not display a stop band. For strained (i.e. ordered) PS latex (diameter, 100 nm) film, an optical stop band is observed at 600 nm. The experimentally observed absorption band is close to the theoretical value (i.e. 670 nm). The deviation between the measured and calculated values may be explained by factors such as extent of latex ordering and size distribution of latex.

1.4 Elastomeric Conductive Composites

Highly stretchable elastomers with stretch ratios $\lambda > 6$ are of critical importance in solving problems in aerospace, automotive, and petroleum industries [30, 31]. New products of elastomers with enhanced performance are thus needed. The specific challenge in this regard is a quantified target that consists in the optimization of elastomeric-like nanocomposites with multifunctional properties such as monitoring the elastomer strain with electrical resistance variation. The multifunctional performance of these composites is demonstrably high for electroconductive applications as deformable electrode films that can be utilized in a wide variety of electronic devices under high strains. Structurally resilient and electrically conductive composites capable of sustained elongations up to $\lambda = 6$, delivering low sheet resistance, are thus of priority interest.

Valentini et al. [32] recently reported a novel method that consists in the lamination of hydrophobic Parafilm containing graphene nanoplatelets (GNPs) on fluoroelastomer substrate. Once laminated, the Parafilm/GNPs film maintains the electrical resistance reversible under stretch ratios up to $\lambda = 3$. As the composite film was stretched, the resistance was found to increase with the deformation, reaching a maximum value at λ_{max} (i.e. 2 and 3) [7]. Subsequently, as the specimen was brought to the initial state from λ_{max} to 1, the electrical resistance regained the initial values, suggesting an almost reversible mechanism of GNP dragging in the stretch axis direction. For the highest stretch ratio, i.e. $\lambda_{max} = 4$, the resistance did not show any recovery when the sample relaxes to its unstrained condition. This is an indication that at this maximum stretch ratio the electrical network made of GNP contacts is subjected to an irreversible deformation. For filled elastomers, this is known as the Payne effect [33] and has been explained by Kraus [34, 35] via the strain-dependent breaking and reforming of interparticle connections in the filler network. Then, the number density of connections N depends on γ_0 as $N = N_0{}^*[1 + (\gamma_0/\gamma_c)^{2m}]^{-1}$ where N_0 is the initial connection density, m is the network structure factor, and γ_c is the yield strain (Figure 1.6).

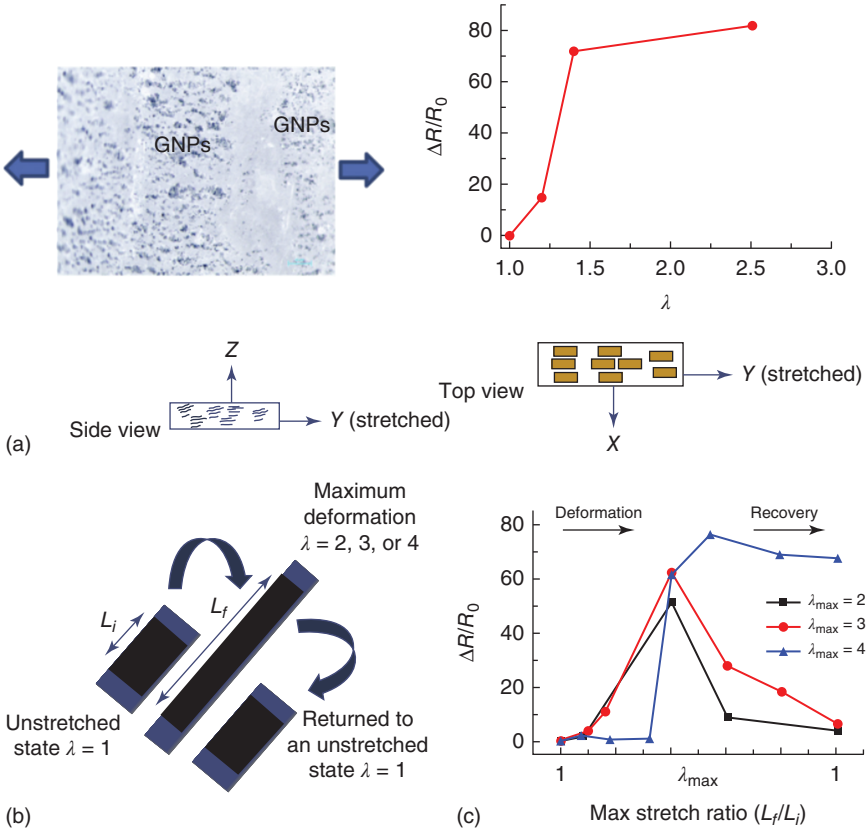

Figure 1.6 (a) Optical micrographs and schematic side/top view of GNP platelets embedded in Parafilm matrix in stretched state (i.e. the arrows indicate the strain direction). The initial side/top view shows an interconnected electrical path of GNPs; GNPs then separate during stretching, thus raising the electrical resistance of the sheet. (b) Schematic representation of stretch mechanism before the stretch at $\lambda = 1$, during the stretch at different stretching ratios, and after relaxing to an unstretched state $\lambda = 1$ of Parafilm/GNPs coupled with fluoroelastomer. (c) Electrical resistance variations to initial resistance values of Parafilm/GNPs coupled with fluoroelastomer substrate through the stretching cycles from $\lambda = 1$ to $\lambda_{max} = 2$, 3, or 4, and then returned to a relaxed state ($\lambda_{max} = 1$).

Referring to the experiment reported in ref. [32], it was also demonstrated that the strain, after which the delamination occurs, can be used to calculate the adhesion energy according to a model where the film can be considered as an adhesive tape with tension attached to a substrate [36]. From such a theory of peeling for large deformations in strained conditions, the strain for film delamination ($\lambda_d = 4$) can be expressed in terms of adhesion energy (G), film's Young modulus (E), and film thickness (t) as $\ln(\lambda_d) = 2\ (G/Et)^{0.5}$, which, for $E = 0.0063$ MPa (see ref. [32]) and $t = 140\,\mu$m, restitutes a value of $G \sim 0.41$ N m^{-1}. This simple example indicates that the critical value of film delamination found for the composite coating on elastomeric substrate coincides with that measured at rupture for the coating, suggesting that the substrate makes mechanical behavior

of the coating reversible until its rupture despite the plastic deformation of the viscoelastic film.

1.5 Conclusions and Future Perspectives

This chapter is intended to supply recent advances on the fundamental mechanical properties of soft composites for applications in stretchable devices as well as providing descriptions of devices including those based on polymers and graphene as active components. Particular attention has been focused on the processing and integration of carbon-based materials in multifunctional composites. We demonstrate how by controlling the microscopic order of such composite films with a simple stretch, one can develop new multifunctional materials with nanoscale mechanisms visible at the macroscale. The coupling of elastic and stiff platelets such as graphene oxide with viscoelastic polymer matrix enables the reversible control of the morphologies as well as the electrical resistance of the composite coating. Disordered nanoparticles should have improved degrees of ordering in the stretched sample by shear forces and this can produce change of colors under strain. Finally, we present novel, electrically conductive, adherent composites that are capable of sustaining severe elastic deformation and recoverable electrical performance.

Acknowledgments

NMP is supported by the European Research Council (ERC PoC 2015 SILKENE nr. 693670) and by the European Commission H2020 under the Graphene Flagship (WP14 "Polymer composites," n. 696656) and under the FET Proactive ("Neurofibres" no. 732344).

References

1 Brook, I., Mechrez, G., Suckeveriene, R.Y. et al. (2013). A novel approach for preparation of conductive hybrid elastomeric nanocomposites. *Polym. Adv. Technol.* 24: 758–763.
2 Kim, K.-S., Jung, K.-H., and Jung, S.-B. (2014). Design and fabrication of screen-printed silver circuits for stretchable electronics. *Microelectron. Eng.* 120: 216–220.
3 Woo, S.-J., Kong, J.-H., Kim, D.-G., and Kim, J.-M. (2014). A thin all-elastomeric capacitive pressure sensor array based on micro-contact printed elastic conductors. *J. Mater. Chem. C* 2: 4415–4422.
4 Dalmas, F., Cavaille, J.-Y., Gauthier, C. et al. (2007). Viscoelastic behavior and electrical properties of flexible nanofiber filled polymer nanocomposites. Influence of processing conditions. *Compos. Sci. Technol.* 67: 829–839.
5 Shin, M.K. et al. (2010). Elastomeric conductive composites based on carbon nanotube forests. *Adv. Mater.* 22: 2663–2667.

6 Chun, K.-Y. et al. (2010). Highly conductive, printable and stretchable composite films of carbon nanotubes and silver. *Nat. Nanotechnol.* 5: 853–857.

7 Schutzius, T.M., Tiwari, M.K., Bayer, I.S., and Megaridis, C.M. (2011). High strain sustaining, nitrile rubber based, large-area, superhydrophobic, nanostructured composite coatings. *Composites Part A* 42: 979–985.

8 Vosgueritchian, M., Lipomi, D.J., and Bao, Z. (2012). Highly conductive and transparent PEDOT:PSS films with a fluorosurfactant for stretchable and flexible transparent electrodes. *Adv. Funct. Mater.* 22: 421–428.

9 Gao, H.J., Ji, B.H., Jager, I.L. et al. (2003). Materials become insensitive to flaws at nanoscale: Lessons from nature. *Proc. Natl. Acad. Sci. U. S. A.* 100: 5597–5600.

10 Buehler, M.J. and Yung, Y.C. (2009). Deformation and failure of protein materials in physiologically extreme conditions and disease. *Nat. Mater.* 8: 175–188.

11 Yang, W., Sherman, V.R., Gludovatz, B. et al. (2015). On the tear resistance of skin. *Nat. Commun.* 6: 6649.

12 Buehler, M.J., Keten, S., and Ackbarow, T. (2008). Theoretical and computational hierarchical nanomechanics of protein materials: deformation and fracture. *Prog. Mater. Sci.* 53: 1101–1241.

13 (a) Park, S.H. and Xia, Y. (1999). Assembly of mesoscale particles over large areas and its application in fabricating tunable optical filters. *Langmuir* 15: 266. (b) Tran, P. (1997). Optical limiting and switching of short pulses by use of a nonlinear photonic bandgap structure with a defect. *J. Opt. Soc. Am. B* 14: 2589.

14 Vogelaar, L., Nijda, W., van Wolferen, H.A.G.M. et al. (2001). Large area photonic crystal slabs for visible light with waveguiding defect structures: fabrication with focused ion beam assisted laser interference lithography. *Adv. Mater.* 13: 1551.

15 Lopez, C. (2003). Materials aspects of photonic crystals. *Adv. Mater.* 15: 1679.

16 Chen, L.B., Ackerson, B.J., and Zukoski, C.F. (1994). Rheological consequences of microstructural transitions in colloidal crystals. *J. Rheol.* 38: 193–216.

17 Ciamarra, M.P., Coniglio, A., and Nicodemi, M. (2005). Shear instabilities in granular mixtures. *Phys. Rev. Lett.* 94: 1–4.

18 Ackerson, B.J. (1988). Shear-induced order in suspensions of hard spheres. *Phys. Rev. Lett.* 61: 1033–1036.

19 Fan, Y. and Hill, K.M. (2011). Phase transitions in shear-induced segregation of granular materials. *Phys. Rev. Lett.* 106: 1–4.

20 Pusey, P.N. and van Megen, W. (1986). Phase behaviour of concentrated suspensions of nearly hard colloidal spheres. *Nature* 320: 340–342.

21 Terentjev, E. (2002). Searching for equilibrium. *Nat. Mater.* 1: 149–150.

22 Menut, P., Seiffert, S., Sprakel, J., and Weitz, D.A. (2012). Does size matter? Elasticity of compressed suspensions of colloidal- and granular-scale microgels. *Soft Matter* 8: 156.

23 Snoswell, D.R.E. et al. (2010). Shear ordering in polymer photonic crystals. *Phys. Rev. E* 81: 2–5.

24 Zhao, Q. et al. (2016). Large-scale ordering of nanoparticles using viscoelastic shear processing. *Nat. Commun.* 7: 11661.

25 López Jiménez, F., Upadhyaya, P., Liljenhjerte, J. et al. (2016). *Extreme Mechanics Letters* 9: 297–303.

26 Hure, J., Roman, B., and Bico, J. (2011). Wrapping an adhesive sphere with an elastic sheet. *Phys. Rev. Lett* 106: 174301.

27 Suk, J.W., Piner, R.D., An, J., and Ruoff, R.S. (2010). Mechanical properties of monolayer graphene oxide. *ACS Nano* 4 (11): 6557–6564.

28 Gu, Z.Z., Fujishima, A., and Sato, O. (2002). Fabrication of high-quality opal films with controllable thickness. *Chem. Mater.* 14: 760.

29 Miguez, H., Lopez, C., Meseguer, F. et al. (1997). Photonic crystal properties of packed submicrometric SiO_2 spheres. *Appl. Phys. Lett.* 71: 1148.

30 Rooj, S., Das, A., and Heinrich, G. (2011). Tube-like natural halloysite/fluoroelastomer nanocomposites with simultaneous enhanced mechanical, dynamic mechanical and thermal properties. *Eur. Polym. J.* 47: 1746–1755.

31 Kader, M.A., Lyu, M.Y., and Nah, C. (2006). A study on melt processing and thermal properties of fluoroelastomer nanocomposites. *Compos. Sci. Technol.* 66: 1431.

32 Valentini, L., Bittolo Bon, S., Mussolin, L. et al. (2017). Development of conductive paraffin/graphene films laminated on fluoroelastomers with high strain recovery and anti-corrosive properties. *Compos. Sci. Technol.* 149: 254.

33 Payne, A.R. (1962). The dynamic properties of carbon black-loaded natural rubber vulcanizates. Part I. *J. Appl. Polym. Sci.* 6: 57–63.

34 Heinrich, G. and Kluppel, M. (2002). Recent advances in the theory of filler networking in elastomers. *Adv. Polym. Sci.* 160: 1–44.

35 Kraus, G. (1984). *J. Appl. Polym. Sci. Symp.* 39: 75–92.

36 Pugno, N.M. (2011). The theory of multiple peeling. *Int. J. Fract.* 171: 185–193.